

Strain-based critical plane approach to predict the fatigue life of high frequency mechanical impact (HFMI)-treated welded joints depending on the material condition

Jan Schubnell¹ · Volker Hardenacke¹ · Majid Farajian¹

Received: 26 August 2016 / Accepted: 11 July 2017 / Published online: 28 August 2017
© International Institute of Welding 2017

Abstract After post-treatment with high frequency impact treatment (HFMI) of weld toes, a significant increase of fatigue strength or fatigue life can be achieved. Due to the lack of methods for the quantitative prediction of the HFMI benefits depending on the process and treated material, a widespread use of this process has not yet happened. One reason for that issue is that at the moment, no methods exist to predict the influence of the HFMI-treatment on welded components and structures at the moment in advance depending on the HFMI-treatment parameters. For this case, a strain-based approach based on the finite element (FE) simulation of the HFMI-process and the subsequent evaluation by critical plane approaches of the FE-post-processing was developed. This approach principally considers the beneficial effects of compressive residual stresses, notch effect reduction, and hardening of the HFMI-treated surface layer. Furthermore, residual stress relaxation during fatigue loading was taken into account. For numerical prediction of the influence of HFMI-treatment of welds, process parameters at the real device were measured and a suitable material hardening model was used from previous work to describe the conditions in the surface layer. After this, the process chain of welding, HFMI-treatment, and fatigue

loading of butt joint specimen were simulated. The estimated fatigue life values were compared with the values of the fatigue tests for two different treatment intensities and also a good agreement was reached.

Keywords (IIW Thesaurus) Welding · Fatigue strength improvement · High frequency mechanical impact (HFMI) treatment · Finite element simulation · Critical plane approaches

Nomenclature

σ_{nA}	Normal stress amplitude
$\Delta\varepsilon_n$	Normal strain range
E	Young's modulus
R	Load ratio
σ'_f	Fatigue strength coefficient
ε'_f	Fatigue ductility coefficient
b	Fatigue strength exponent
c	Fatigue ductility exponent
E_m	Welding energy per unit length
V	Welding speed
f_f, a_r	Parameter of Goldak heat source
FAT	Fatigue strength at 2×10^6 cycles and failure probability of 2.3%
$\Delta\gamma$	Shear strain range
$\Delta\sigma_n$	Normal stress range
σ_y	Yield strength
τ_f	Shear fatigue strength coefficient
γ_f	Shear fatigue ductility coefficient
G	Shear modulus
b_γ	Shear fatigue strength exponent

Recommended for publication by Commission XIII - Fatigue of Welded Components and Structures

✉ Majid Farajian
majid.farajian@iwm.fraunhofer.de

¹ Fraunhofer Institute for Mechanics of Materials IWM, Freiburg, Germany

c_γ	Shear fatigue ductility exponent
k	Material constant (FS-model)
h	Radiative heat loss
T_0	Ambient air temperature
m	Inverse slope of S-N curve

1 Introduction

The advantages of removing the potential threats of unwanted (tensile) residual stresses and exploiting the beneficial (compressive) residual stresses by mechanical treatments are already known in welding communities. The innovation of locally modifying the residual stress state in welded components by the use of an ultrasonic hammering technology is widely attributed to E. Statnikov [1]. Nowadays, there are different HFMI tool manufacturers and service providers, but the operating principle is always identical: an indenter is accelerated against a component's surface with high frequency, causing local plastic deformation and residual stresses.

In this context, high frequency hammer peening as post-weld treatment is a statistically proven method to increase the fatigue life of welded joints [2–13]. During this process, a hardened cylindrical metal pin with a spherical tip impacts the weld toe surface with high frequency and induces local plastic deformation. The resulting surface compressive residual stresses, the reduced notch effect at the weld toe, and the local work hardening of the material are the main reasons for the increased fatigue strength [13, 14]. The interactions between these effects and their single influence to the fatigue strength improvement of HFMI-treated welded joints are still not completely understood. The presented approach in this work considers all these three effects. However, a final conclusion of which effect has the highest influence could not certainly be made.

The benefit of HFMI-treatment was quantified by numerous experimental fatigue tests and statistical evaluation [4–6] according to the established stress-based methods: nominal stress approach, structural stress approach, and notch stress approach according to the fatigue design recommendations of the International Institute of Welding (IIW) for untreated welded joints [15]. These approaches have already been applied with success for different steel grades [16]. Former studies show that the fatigue life prediction by strain-based approaches is also a suitable method but needs more information about material behavior and geometry of the fatigue relevant zone [17, 18]. Numerical investigations of HFMI-treated S700MC steel showed that material behavior, especially the residual stress state and residual stress stability, have high influence on the fatigue damage of HFMI-treated welded joints [19, 20].

To predict the increase of fatigue life by damage and fracture mechanical local approaches, it is absolutely necessary that the numerical calculations describe the induced residual stress field accurately. Recent work in this field focused on the influence of the mesh size, choice of friction model, overlapping of tool indentations, and applicable boundary conditions on the numerical simulations [21–27].

Currently, no approach exists that predict the fatigue behavior of HFMI-treated welded joints depending on the parameter of the HFMI-process (treatment intensity). For this, it is necessary to describe the material condition in the HFMI-treated surface layer (hardness, residual stress) and consider additionally the modification of the weld toe geometry. The presented approach in the hand shows one possibility for fatigue life prediction of HFMI-treated welded joints based on a mixture of the experimental measurements and finite element analysis.

2 Critical plane approaches

The field of damage mechanics describes the crack initiation and micro crack growth up to a determined macro crack length (on the order of 1 mm in depth). Crack propagation cannot be described with this approach and is neglected in this study. Investigations [28, 29] illustrate that crack initiation is dominant for the investigated high cycle fatigue regime and can cover around 90% of the total fatigue life. Investigations on welded joints by [30, 31] show that crack initiation life is an unneglectable part of the total life even for high strength steels. Furthermore, experimental investigations on butt joint specimen made of different structural steel grades show that the crack initiation portion depends on the steel grade and can reach more than 80% of the total fatigue life for $N_f > 10^5$ cycles [32, 33]. According to this, two damage mechanic models were used in this study considering different types of micro crack growth.

2.1 Smith-Watson-Topper model

First, for tensile-mode of cracking, the model of Smith, Watson, and Topper [34] was used:

$$\sigma_{nA} \frac{\Delta \varepsilon_n}{2} = \frac{\sigma_f^2}{E} (2N)^{2b} + \sigma_f' \varepsilon_f' (2N)^{b+c} \quad (1)$$

where σ_{nA} is the normal stress amplitude and $\Delta \varepsilon_n$ is the normal strain range according to the evaluation plane and E is the Young's modulus of elasticity, describing damage as a reason of axial strain. The damage (left side of eq. 1) correlates with the number of cycles to crack initiation N according to the correlation proposed by [35] (right side of eq. 1) as mean

stress correction of the original definition. The strain-life fatigue properties σ'_f , ϵ'_f , b , and c must be determined from uniaxial fatigue tests on the investigated material.

2.2 Fatemi-Socie model

Second used model describes shear-mode cracking according to Fatemi and Socie [36]:

$$\frac{\Delta\gamma}{2} \left(1 + k \frac{\sigma_{nA}}{\sigma_y} \right) = \frac{\tau_f^2}{G} (2N)^{2b_\gamma} + \gamma'_f (2N)^{c_\gamma} \tag{2}$$

where $\Delta\gamma$ is the shear strain range and σ_{nA} is the normal stress amplitude according to the evaluation plane, G is the shear modulus, σ_y is the monotonic yield strength of the material, and k is a material constant reflecting the sensitivity of the material to normal mean stress. Furthermore, k increases with an increasing number of cycles [36–38]. As first, conservative approximation it is proposed to set $k=1$ and $\sigma_y = \sigma'_f$ [36]. The damage (left side of eq. 2) correlates with the number of cycles to crack initiation N according to the strain-life properties τ'_f , γ'_f , b_γ , and c_γ for shear. The constants for axial strain (right side of eq. 1) and for shear (right side of eq. 2) can be translated to each other $\sigma'_f = \sqrt{3}\tau'_f$, $\gamma'_f = \sqrt{3}\epsilon'_f$, $b \approx b_\gamma$ and $c \approx c_\gamma$ according to [38].

If no fatigue data for the determination of the strain-life properties is available, some simple approximation by Roessle and Fatemi [37] can be used. For this fatigue strength, exponent b is set to -0.09 and the fatigue ductility exponent c is set to -0.60 . These are average values for steel. A good correlation of the fatigue strength coefficient σ'_f in MPa with the Brinell hardness (HB) is given by the following equation:

$$\sigma'_f = 4.25 \text{ HB} + 225 \tag{3}$$

Also, a good correlation between the fatigue ductility coefficient ϵ'_f and the Brinell hardness is given by the second order polynomial:

$$\epsilon'_f = \frac{0.32 \text{ HB}^2 - 487 \text{ HB} + 191000}{E} \tag{4}$$

This approximation is valid for high cycle fatigue for steels with Brinell hardness of $150 < \text{HB} < 750$. For low and medium carbon steels, like SAE 1050, SAE 1090, and SAE 1541, the approximation shows a very good agreement. This approximation was extended by Shamsaei and Fatemi [39] to multiaxial fatigue. For this, the von Mises criterion was used correlating eq. 2 with eq. 3 and eq. 4 by translating the strain-

life properties for axial strain to shear with $\sigma'_f = \sqrt{3}\tau'_f$, $\gamma'_f = \sqrt{3}\epsilon'_f$ with $E = 200$ GPa. This finally leads to the following equation:

$$\begin{aligned} \frac{\Delta\gamma}{2} \left(1 + k \frac{\sigma_{nA}}{\sigma_y} \right) &= \frac{6.37 \text{ HB} + 338}{200000} (2N)^{-0.09} \\ &+ \frac{0.55 \text{ HB}^2 - 842 \text{ HB} + 331000}{200000} (2N)^{-0.056} \end{aligned} \tag{5}$$

As mentioned, k depends on the number of cycles N . An approximation of k by HB and N is also given by [39] as followed:

$$k = (0.0003 \text{ HB} + 0.0585 \text{ HB})(2N)^{0.09} \tag{6}$$

Investigations made by [37–39] show high crack initiation predictability with an acceptable scatter of ± 3 .

3 Numerical fatigue life calculation approach

Figure 1 shows principle procedure of the fatigue life calculation approach in this study. This approach contains stepwise simulation of the process specimen manufacturing, HFMI-treatment, fatigue loading, and finally, the damage mechanics evaluation. For experimental validation, welded specimens were manufactured and tested under fatigue loading.

For the fatigue life prediction, it is necessary to describe the HFMI-process and the resulting residual stress field accurately. In previous studies, the influence of the numerical parameters was investigated [21]. Then, investigations were performed to describe the HFMI-induced residual stress field in the surface layer for flat steel specimen of S355 [26, 27]. Furthermore, the characterization of the base material S355J2H with tensile and incremental tests was performed by former investigation [26]. This shows a good agreement with experimental measured residual stress profiles with X-ray and neutron diffraction techniques.

3.1 Experimental work

Totally, 36 MAG-welded specimens were manufactured made of S355J2H. The weld type was a two-layer butt weld. Fifteen specimens stayed in as-welded (AW) condition for reference. The others were treated with an ultrasonic impact treatment (UIT) device of the company SONATS [40]. This UIT-device contains an ultrasonic-frequency generator for controlling and adjustment of the excitation frequency, a sonotrode that converts electrical vibration into mechanical vibration, a pin holder, and a pin that perform the impacts. The radius of the used intender pin was 1.5 mm. The amplitude of the sonotrode A can be adjusted from $A = 10 \mu\text{m}$ (low intensity) to $A = 60 \mu\text{m}$

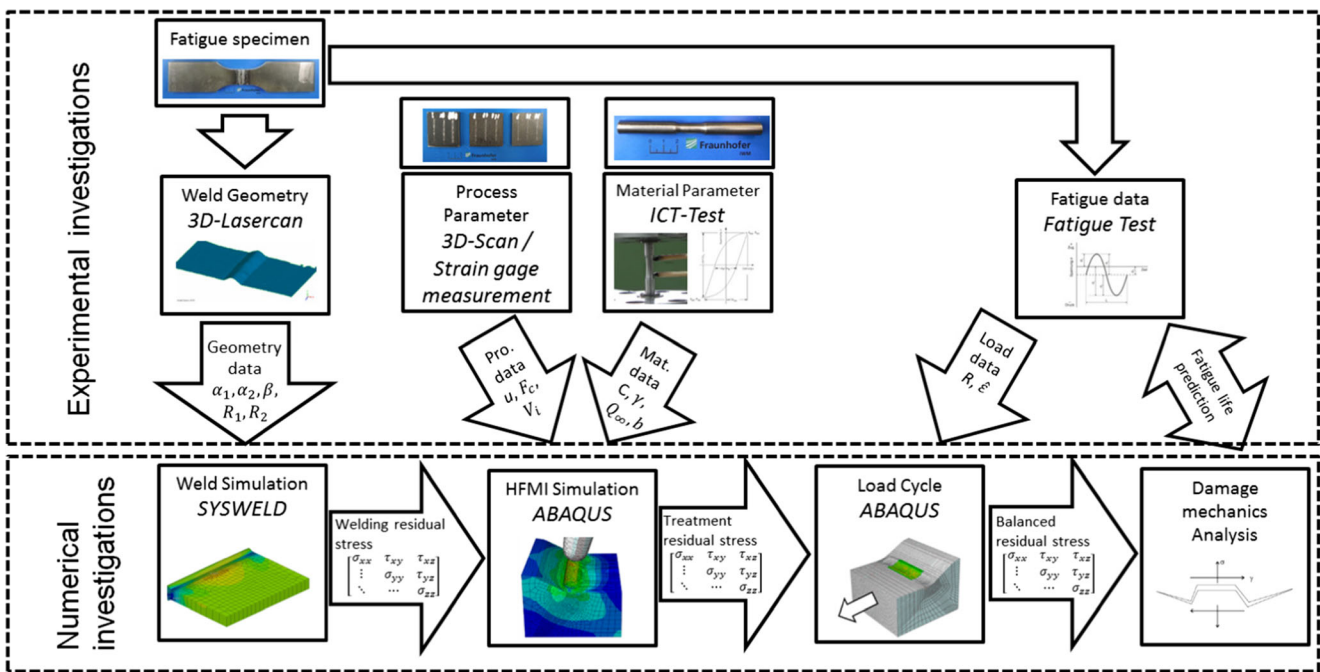


Fig. 1 Fatigue life calculation approach

(high intensity). Amplitude of 60 μm is recommended by the device manufacturer for steel application. According to this, 15 specimens were treated with the amplitude of $A = 60 \mu\text{m}$ and 6 specimens were treated with a lower intensity of $A = 30 \mu\text{m}$, to show if differences in fatigue life based on the HFMI treatment intensity could be overserved.

The fatigue test was performed with a high frequency generator, type HFP5100 of the company ZWICK with a maximum force of 150 kN. The testing frequency was 100 Hz and the shut-down criterion was a decrease of 2 Hz in the testing frequency.

After treatment, the specimen surface geometry was digitalized with a 3D-laser scanner. The geometrical accuracy of the measuring system is $\pm 5 \mu\text{m}$. Similar techniques and surface preparations as [41, 42] were used. Then, the geometrical parameters flank angle α , angle of distortion β , weld toe radius R_{AW} in AW condition, and R_{HFMI} in HFMI-treated condition were evaluated. All values are summarized in Table 1. The permanent indentation depth u is defined as the vertical distance between the bottom of the HFMI-treated notch and a plane of the metal sheets in a distance of 0.5 to 5 mm of the weld toe.

The geometrical values in this case follow the normal distribution. The weld toe radius was determined by least square fit of a circle at the weld toe, illustrated in Fig. 2. Due to inaccuracy by selecting the area for the least square fit, this procedure was repeated 6 times at different positions on each weld toe. The weld toe radius of each specimen was averaged about 6 measurements. As shown, the mean weld toe radius in HFMI-treated condition is smaller than in AW condition. Assuming that locations with very small weld toe radii lead to crack initiation, it cannot be concluded that the reduction of the notch effect is not a crucial part for the HFMI-treatment benefit. Shape and size of the welded zone and the heat-affected zone (HAZ) were evaluated from grinded cross sections. It shows that the width of the HAZ is between 1.5 to 2 mm.

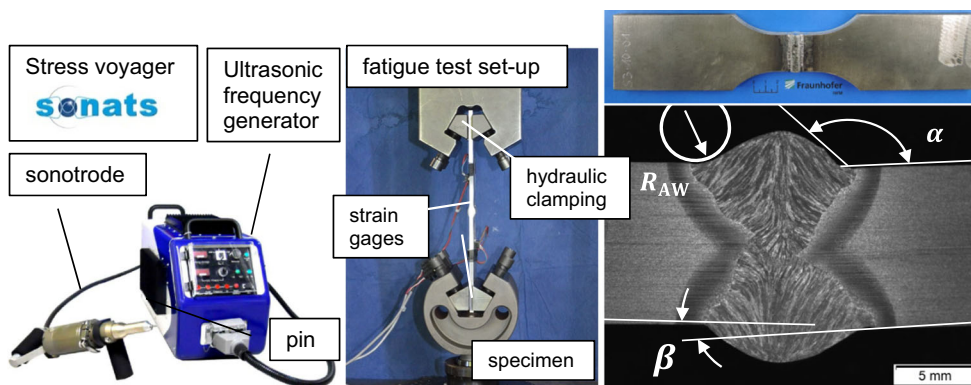
3.2 Welding simulation

The simulation of the MAG-welding process was performed with the commercial software SYSWELD©, executing the welding process and decoupled thermal and mechanical simulation. A complete metal sheet with the length of 100 mm, width of 75 mm, and thickness of 10 mm was modeled as a half-model

Table 1 Values and standard deviation (s) of dimensions fort butt weld specimen

	as-welded (AW)			HFMI $A = 30 \mu\text{m}$		HFMI $A = 60 \mu\text{m}$	
	α [°]	β [°]	R_{AW} [mm]	u [mm]	R_{HFMI} [mm]	u [mm]	R_{HFMI} [mm]
Mean value	152.25	0.48	2.56	0.131	1.467	0.172	1.756
s	5.24	0.57	1.36	0.053	0.297	0.052	0.168
specimen	15	15	15	15	15	6	6

Fig. 2 *Left:* UIT-device of the company SONATS [SONATS], *middle:* Fatigue test set-up for welded specimen, and *right:* butt weld specimen and evaluated geometrical parameters



using the YZ-symmetry plane, shown in Fig. 3. As material-hardening model, the internal data of SYSWELD© of S355J2G3 was used, contains isotropic hardening [43]. The ellipsoid heat source according to Goldak [44] was chosen as heat input. As cooling down boundary condition, free air convection was used, with a cooling time of each weld pass from 1800 s. The welding simulation parameters are summarized in Table 2.

The results showed tensile residual stresses in transverse direction of the weld of 210 MPa at the weld toe of the second welding pass in the middle of the specimen. The welding residual stresses in other direction at the surface are significantly lower.

Residual stress measurements performed with X-ray diffraction at six similar butt weld specimen show that tensile welding residual stress at five specimen from 170 to 40 MPa exist at the weld toe in transverse direction. The specimen with the highest tensile residual stress is shown in Fig. 3. The measured residual stresses in longitudinal directions in every specimen are significantly lower. The welding residual stress seems also to be the worst case and was used for a conservative fatigue estimation of the HFMI-treatment benefit.

In the next step, the calculated welding residual stress field was transferred to ABAQUS©. For that, stress tensors and equivalent plastic strains were linearly interpolated from nodes in SYSWELD© to Gaussian integration points of the FE-elements in ABAQUS©. Differences occur because of different mesh size which is around 10 times smaller in ABAQUS©. The

minimum size of the elements at the weld toe in ABAQUS was 100 μm . Due to node-based interpolation of the stress values, differences of around 10% occurs, shown in Fig. 4, which has been considered to be acceptable for this study. Comparisons with multiple X-ray diffraction measurements show that the transferred residual stress in ABAQUS© show a high agreement with the experimental determined residual stress values.

3.3 Simulation of the HFMI-treatment

The simulation of the HFMI-treatment was performed according to former studies of [21, 26, 27]. The same hardening model and simulation procedure were used than for the numerical investigation of flat S355J2H base material specimen [26] using non-linear combined isotropic-kinematic hardening with strain rate dependency according to the back-stress law of [45–47]. The isotropic part of the material model was defined by tabular data, which makes it possible to define material properties for large plastic deformations. Base material behavior is assumed for the treated area. For a more efficient simulation, the geometry was divided into two parts. One with a fine mesh with a minimum element edge size of 100 μm and totally 43,520 C3D8R elements and a second part with a minimum elements size of 2 mm and totally 12,026 elements. Tie connectors were used for the connection. Since fatigue strength follows the weakest link, the combination of measured geometrical values

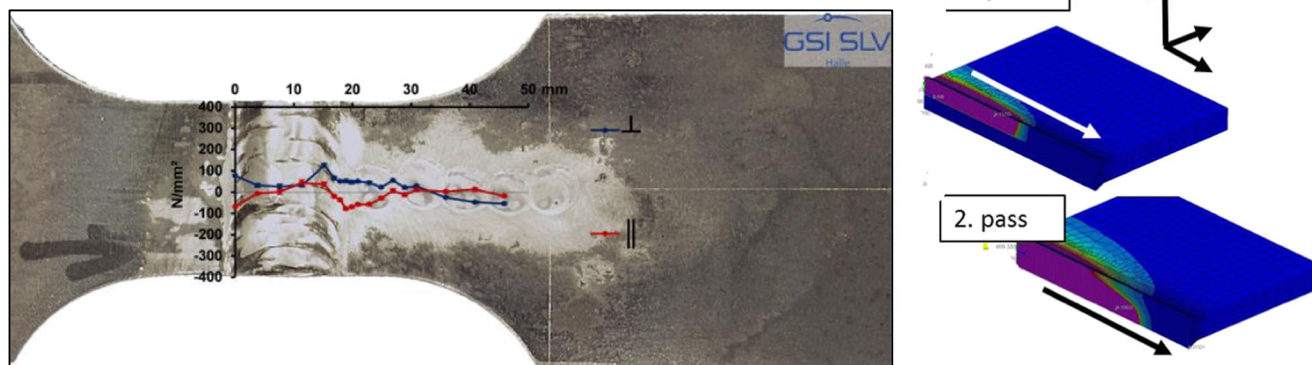
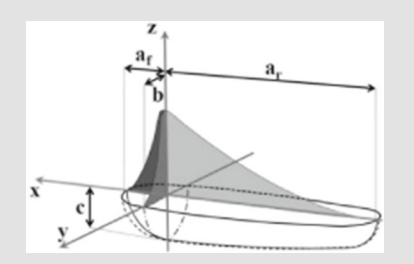


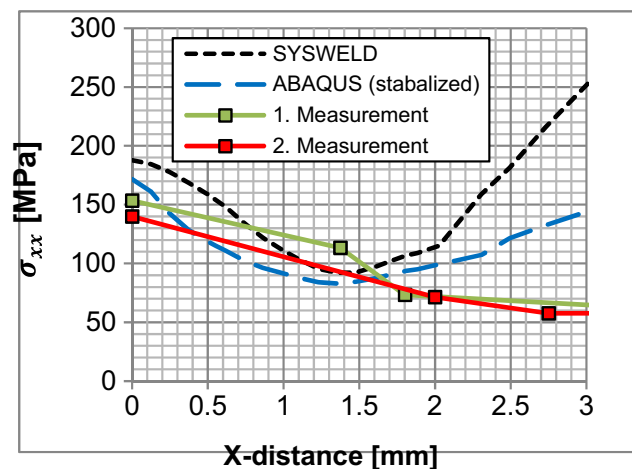
Fig. 3 Residual stress measurement at butt joint specimen and simulation of the welding process

Table 2 Parameter for welding simulation with heat source according to [44]

E_m [J/mm]	V [mm/s]	f_f [-]	a_f [mm]
1130	8.833	1.2	5.333
b [mm]	c [mm]	h [W/m ²]	T_0 [K°]
6	6	25	20



expecting the highest stress concentration factor was used to model the weld toe. Assuming a normal distribution about the measured geometrical values in Table 1, the weld toe radius R_{AW} in the model was set to 1.2 mm and the flank angle α to 147° meaning that 68.3% of the specimen had lower stress concentration factors. Two simulations were performed, one assuming a low HFMI-treatment intensity ($u=0.131$ mm) and one assuming high intensity treatment ($u=0.171$ mm). The simulations were performed displacement controlled in three steps with 70, 85, and 100% of the total indentation depth. The impact speed of the pin was set to 3.5 m/s. Due to the elastic response of the material, an additional displacement of the pin of 15% is needed to reach the exact permanent indentation depth. These simulation procedure was determined empirically. A limited number of 75 impacts (25 for each simulation step) were simulated with a distance between the steps of 0.4 mm [21, 24]. Figure 5 shows the simulation of the HFMI-process. In the contour plot, it is illustrated that nearly all welding residual stresses were completely eliminated during the HFMI-process. The evaluation of the residual stresses after treatment shows that the surface stress in transverse direction σ_{xx} in the middle of the treated area are around -270 MPa for low intensity treatment and around -460 MPa for high intensity treatment. Not considering the influences of the welding residual stress field in

**Fig. 4** Comparison of simulated and experimental measured residual stress values by X-ray diffraction

the simulation lead to approximately 15% higher surface compressive residual stresses.

However, it should be noticed that the inhomogeneity of the surface residual stress state after the HFMI-treatment simulation is very high. The stress values of single elements differ partially around $\pm 50\%$ of the average values. The stress values of single elements are also close to zero. It is strongly recommended to average the stress values for each evaluation within a certain volume. In this case, the residual stresses are averaged over 25 elements ($0.5 \text{ mm} \times 0.5 \text{ mm}$) in each evaluation layer.

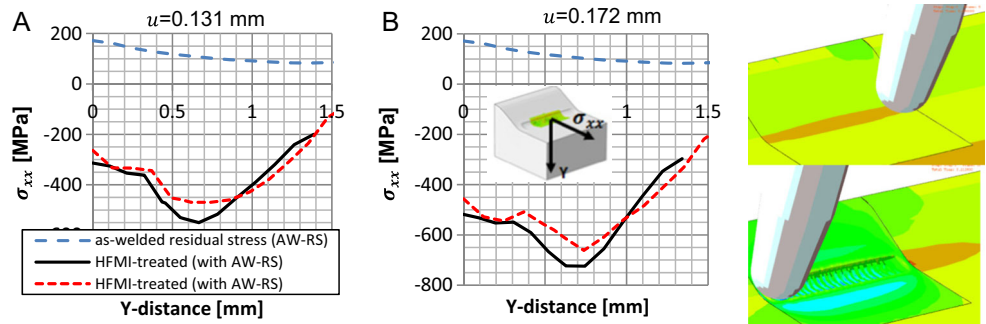
3.4 Simulation of the cyclic fatigue loading

The simulation of the fatigue load attends to perform damage mechanic evaluation for fatigue assessment. For this, one load cycle which is representative for the complete fatigue life is theoretically enough. In this case, five load cycles were simulated for two reasons: firstly, to stabilize the inhomogeneous residual stress field and secondly, to consider the effect of residual stress relaxation. The stress relaxation of untreated welded joints of different steel grades were experimentally investigated by [48], showing that residual stress relaxation can be expected for low strength steel grade S355. The relaxation of HFMI-induced residual stresses was investigated by [49, 50].

Figure 6 shows that for cyclic loading with a stress ratio $R=0.1$ and a maximum load stress of 80% of the yield strength of the base material relaxation of ± 100 MPa occurs. If only low HFMI-induced surface residual stresses from -100 to -150 MPa exist, they could relax fully. In this study, no experimental investigations about residual stress relaxations were made.

Figure 6 shows the principle procedure for the fatigue load simulation. The load was simulated stress-controlled with default nominal stress ranges $\Delta\sigma_n$ of 315, 290, 245, 220, and 225 MPa with the load ratio R of 0.1. These stress ranges are the stress ranges for the fatigue testing of the real samples. It could also be observed that residual stress relaxation for all load levels leads to the relaxation of a similar percentage of the initial residual stresses. Evaluating the residual stresses in transverse direction after the fifth load cycle shows that relaxation of around 50% of the original residual stress value may occur under very high load amplitudes. However, it is unclear if the

Fig. 5 Simulation of the HFMI-process of the butt weld treatment and the induced transversal induced residual stresses σ_{xx} for low intensity treatment (a) and for high intensity treatment (b)



relaxation of the numerical inhomogeneity or the physical phenomena of residual stress relaxation have a higher contribution.

3.5 Damage mechanic evaluation

After the simulation of the HFMI-treatment, the fatigue life analyses of the welded joint at different locations were performed. For this, the damage parameter (left side of eq. 1 and eq. 2) were evaluated based on the FE-post-processing (Gaussian integration points of finite elements). Similar fatigue life analyses were performed before by [51, 52]. The principle of the critical plane was used, assuming that the fatigue life is determined by highest damage occurring on an evaluation plane a so-called critical plane. To achieve a representative stress state for evaluation, the stress at the surface was averaged within a volume X/Y/Z of 0.5 mm × 0.5 mm × 0.2 mm. Those are totally 50 elements. Investigations in this work showed that a higher

volume do not lead to significant difference for the averaged residual stress state. However, smaller volume showed high differences on the residual stress state depending on the locations of evaluation. Then, the base vectors of the stress tensor $\sigma = [\sigma_{xx}, \sigma_{yy}, \sigma_{zz}, 2\sigma_{xy}, 2\sigma_{xz}, 2\sigma_{yz}]$ at maximum load and strain tensor at minimum load $\epsilon' = [\epsilon'_{xx}, \epsilon'_{yy}, \epsilon'_{zz}, 2\gamma'_{xy}, 2\gamma'_{xz}, 2\gamma'_{yz}]$ and maximum load $\epsilon = [\epsilon_{xx}, \epsilon_{yy}, \epsilon_{zz}, 2\gamma_{xy}, 2\gamma_{xz}, 2\gamma_{yz}]$ according to Voigt's notation of each load cycle were turned around the X/Y/Z by the euler angles $\varphi, \Psi,$ and ω by the z,x',z''-convention, according to eq. 3 for stress and eq. 4 for strain values.

$$\sigma' = T^T \sigma T \tag{7}$$

$$\epsilon' = T^T \epsilon T \tag{8}$$

With the coefficient matrices of the tensors $\sigma = \sigma_{ij} e^i \otimes e^j,$
 $\epsilon = \epsilon_{ij} e^i \otimes e^j$

$$\sigma_{ij} = \begin{bmatrix} \sigma_{xx} & \tau_{xy} & \tau_{xz} \\ \tau_{yx} & \sigma_{yy} & \tau_{yz} \\ \tau_{zx} & \tau_{zy} & \sigma_{zz} \end{bmatrix}, \quad \epsilon_{ij} = \begin{bmatrix} \epsilon_{xx} & \gamma_{xy} & \gamma_{xz} \\ \gamma_{yx} & \epsilon_{yy} & \gamma_{yz} \\ \gamma_{zx} & \gamma_{zy} & \epsilon_{zz} \end{bmatrix} \quad T_{kl} = \begin{bmatrix} c(\varphi)c(\omega)-s(\varphi)c(\Psi)s(\omega) & -c(\varphi)c(\omega)-s(\varphi)c(\Psi)s(\omega) & s(\varphi)c(\Psi) \\ s(\varphi)c(\omega)-c(\varphi)c(\Psi)s(\omega) & -s(\varphi)c(\omega) & -c(\varphi)s(\Psi) \\ s(\Psi)s(\omega) & -s(\Psi)s(\omega) & c(\Psi) \end{bmatrix}$$

If the critical plane is found the values stress $\sigma_{nA} = \sigma'_{xx}$ and strain $\Delta\epsilon_n = \epsilon'_{xx} - \epsilon'_{xx}$ values in eq. 1 and $\Delta\gamma = \epsilon'_{xy} - \epsilon'_{xy}$ eq. 2 according to load direction were evaluated and the non-linear equation was solved by N . The principle of the

evaluation of the damage parameter P_{FS} and P_{SWT} by the critical plane approach is shown in Fig. 7. According to [53, 54], the critical plane for brittle materials have an angle of around 90° to load direction and for more ductile materials,

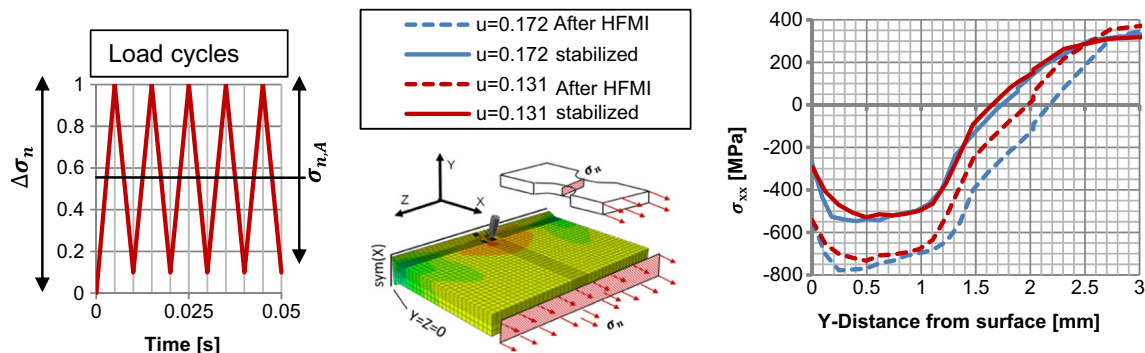


Fig. 6 Fatigue load simulation of the HFMI-process and comparison of HFMI-induced and stabilized residual stress field

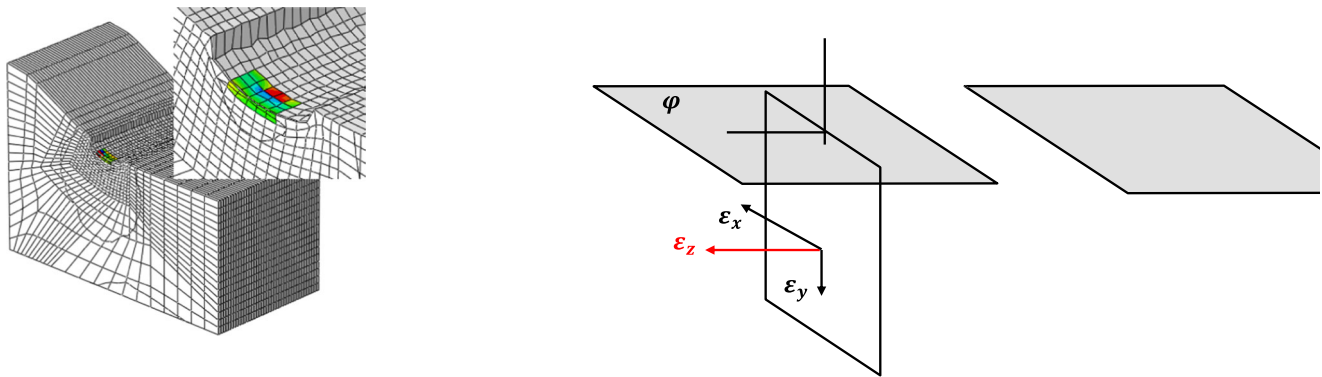


Fig. 7 Evaluation of damage parameters from FE-post processing according to [53]

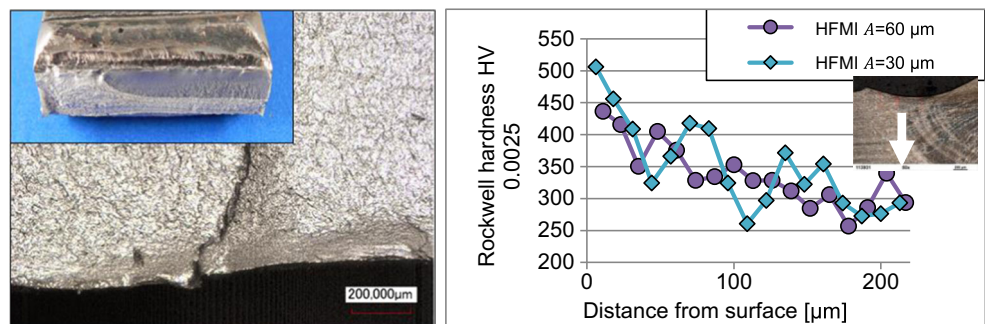
the angle is around 45° degree. Based on this conclusion the fatigue life estimation according to the SWT-model should lead to better correlations for brittle materials and the fatigue life estimation according to the FS-model should lead to better correlations for ductile materials.

The evaluated location was at middle of the treated area at base of the groove. Laser microscope (LM) pictures, shown in Fig. 8, illustrate that crack initiation starts in almost every case at the performed fatigue test exactly at the ground of the groove. The fracture surfaces showed mostly an angle of almost 90° to load direction. However, at some locations, the fracture surface has an angle of around 45° according to load direction in a depth of around $150 \mu\text{m}$.

The strain-life properties for axial strain σ'_f , ϵ'_f , b , and c were determined by the hardness approximation of [37] according to eq. 3 and eq. 4. The strain-life properties for shear τ'_f , γ'_f , b_γ , and c_γ were evaluated according to the approximation of [39]. For this evaluation, hardness measurements of the HFMI-treated surface layer from a depth from of 10 to $220 \mu\text{m}$ were performed for both low and high HFMI-treatment intensities, shown in Fig. 8.

The evaluated hardness values according to Rockwell (HV 0.0025) were averaged about the measured location and translated into Brinell hardness values according to DIN 50150. This leads to hardness values for low amplitude treatment of 333 and to 303 HB for high amplitude treatment. The hardness of the untreated welded material at the weld toe was around 155 HB.

Fig. 8 Laser microscope picture of the fracture surfaces of the HFMI-treated specimen and hardness values measured at the HFMI-treated surface layer



3.6 Comparison between numerical and experimental fatigue data

Figure 9 shows the comparison between experimentally determined S-N curves for the welded specimen in AW condition and in HFMI-treated condition with different treatment intensities and the numerical predicted S-N curves with the critical plane approaches according to the approaches of [34, 36]. It should be mentioned that the failure criterion for the experimental and numerical determined S-N-curves is different. At the experimental test set-up it was final fracture but the critical plane models only consider the crack initiation phase. Therefore, the numerical predicted fatigue values should be clearly conservative compared to the experimental determined ones. The value of k in the FS-model for all calculations was determined according to eq. 6. σ_y was determined according to the approximation of [37] with the measured hardness values according to the different material condition. As shown, this is the case for the evaluated S-N curves in AW condition. In this condition, only the Fatemi-Socie (FS) model was used. The numerical predicted fatigue lives are in average around 53% lower compared with the experimentally determined fatigue lives (failure probability 50%).

For the HFMI-treated conditions, both critical plane models were used. As shown in Fig. 10, the fatigue data evaluated according to the SWT-model is more conservative compared to the FS-model for both treatment intensities. For low intensity, the values determined by the FS-model overestimate the

Fig. 9 Comparison of experimental determined S-N curves with numerical predicted crack initiation curves according to Fatemi-Socie (FS) and Smith-Watson-Topper (SWT) critical plane approach for specimen in as-welded condition (AW), HFMI-treated condition with high intensity ($A = 60 \mu\text{m}$) and HFMI-treated condition with low intensity ($A = 30 \mu\text{m}$)

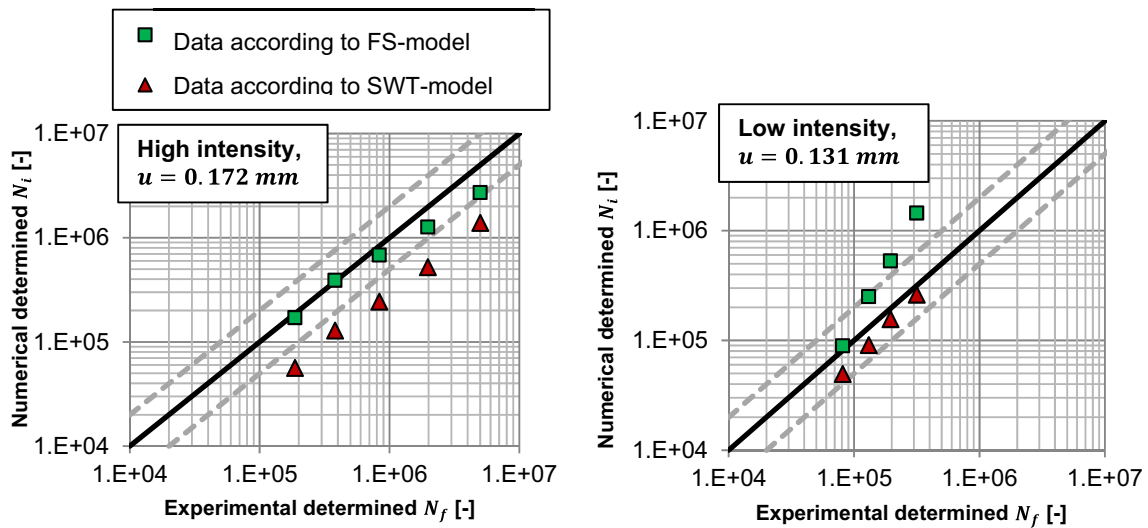
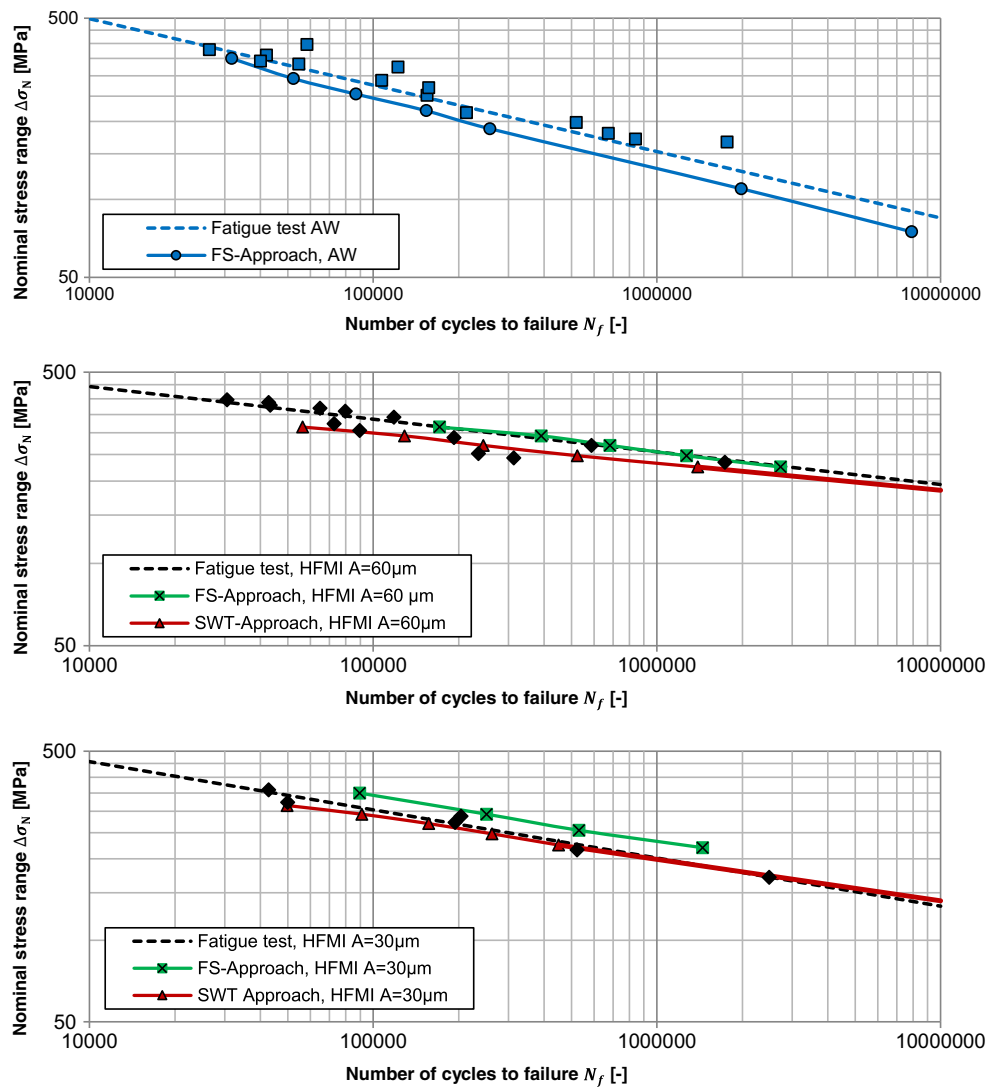


Fig. 10 Comparison of the experimentally determined and numerically determined fatigue life according to the FS-model and according to the SWT-model for high intensity (treatment amplitude $A = 60 \mu\text{m}$, $u = 0.172 \text{ mm}$) and for low intensity (treatment amplitude $A = 30 \mu\text{m}$, $u = 0.131 \text{ mm}$)

fatigue life around 70%. In the case of high intensity, the values vary around $\pm 10\%$ from the experimental determined values. The fatigue assessments by the SWT-approach are conservative by a factor of around 61% for high intensity and around 15% for low intensity from $N_f = 10^4$ to 10^6 cycles and tends to get more optimistic for higher number of cycles.

For a better comparison, the inverse slopes m and the FAT value according to [15, 55] at 2×10^6 cycles for a failure probability of 50% according to the equation:

$$\Delta\sigma_N = \left(\frac{N_E}{N}\right)^{\frac{1}{m}} \text{FAT}$$

were evaluated by least square fit. Where N_E is 2×10^6 .

Independent from the evaluated material condition, the critical plane for the FS-model varied always from $\varphi = +40^\circ$ to $+50^\circ$ ($\Psi = \omega = 0^\circ$) and for the SWT-model from $\varphi = -5^\circ$ to $+10^\circ$ ($\Psi = \omega = 0^\circ$) Table 3.

4 Discussion

It is clear that the measured hardness values with low treatment intensity are higher than for high treatment intensity. This could be caused by a very local measurement only at one position of all HFMI-treated specimens and could explain why the numerical fatigue analysis leads to similar hardness values for both treatment amplitudes.

Figure 10 shows the comparison between the numerical and experimental determined fatigue data. As shown, the fatigue assessment by the SWT-model leads to conservative results, while the FS-model leads to better results for the high intensity case and non-conservative results for the low intensity HFMI-treatment. Reasons can be an overestimated k value in the FS-model or the high hardness values for low intensity treatment. Further investigations needs to be performed to describe the principle mechanism of crack initiation in the HFMI-treated surface layer. Furthermore, the influence of the geometry model approach and evaluation of the hardness values of the high HFMI-treated surface layer was not final investigated. It is

Table 3 Parameters slope (m) and FAT (fatigue value at 2×10^6 cycles) evaluated from experimental and numerical determined S-N curves for AW and HFMI-treated condition with different treatment intensities

	Experimental			Numerical				
	AW	HFMI		AW	HFMI		HFMI	
		A=30 μm	A=60 μm		A=30 μm	A=60 μm	SWT	FS
m	3.9	5.62	8.37	3.8	5.9	6.4	9.4	9
FAT	128	178	235	110	183	240	216	241

assumed that especially the geometry (weld toe radius and flank angle) have a high influence on the simulations results.

5 Conclusion

Calculation of the residual stress field after HFMI is the first step for assessment of the benefits of mechanical surface treatment of the welds. Furthermore, the influence of the advantageous surface material state after such mechanical surface treatment on fatigue is of high importance. The complete process of welding, HFMI-treatment, fatigue loading, and fatigue analysis was performed stepwise for butt joint specimens by numerical simulation and compared to the experimental fatigue test results. The process was performed for specimens in as-welded condition and in HFMI-treated condition with high and low treatment intensities. Damage parameters according to the critical plane models of Smith-Watson-Topper (SWT) and Fatemi-Socie (FS) were evaluated from FE-post-processing from multiple simulations with different load levels. In this way, a complete S-N curve could be calculated. The strain-life properties for both models were determined by the hardness approximation of Roessle and Fatemi. Finally, the numerical and experimental determined S-N curves were compared. This shows that the evaluation according to SWT-model leads to more conservative results than the FS-model in HFMI-treated condition with both intensities. In AW condition, the fatigue analysis with the FS-model leads to clearly conservative fatigue values. A final conclusion which model more suitable for the fatigue life prediction of HFMI-treated welded joints cannot be made.

Generally, all predicted fatigue values are within a scatter band of ± 3 and 80% are within a scatter band ± 2 that is already a good agreement. Furthermore, a significant increase in fatigue life by HFMI-treatment could be numerically determined. Furthermore, it could be numerically shown that higher treatment intensity leads to higher fatigue life. However, further investigations need to be done to quantify the influence of influencing parameters hardness, residual stress stability and evaluation parameters from the FE-analysis on the predicted fatigue life values.

References

1. Statnikov E, Trufyakov V, Mikheev P, Kudryavtsev Y (1996) Specification for weld toe improvement by ultrasonic impact treatment. International Institute of Welding, Paris [IIW Document XIII-1617-96]
2. Yildirim HC, Marquis GB, Barsoum Z (2013) Fatigue assessment of high frequency mechanical impact (HFMI)-improved fillet welds by local approaches. Int J Fatigue 52:57–67

3. Yildirim HC, Marquis GB (2012) Fatigue strength improvement factors for high strength steel welded joints treated by high frequency mechanical impact. *Int J Fatigue* 44:168–176
4. Marquis GB, Mikkola E, Yildirim HC, Barsoum Z (2013) Fatigue strength improvement of steel structures by high-frequency mechanical impact: proposed fatigue assessment guidelines. *Weld World* 57:803–822
5. Marquis G., Barsoum Z., *Fatigue strength improvement of steel structures by high-frequency mechanical impact: proposed procedures and quality assurance guidelines*, welding in the world, DOI 10.1007/s40194-013-0077-8, 2013
6. H. C. Yildirim (2013) Design aspects of high strength steel welded structures improved by high frequency mechanical impact (HFMI) treatment. PhD thesis, Aalto University, Helsinki
7. Yildirim HC, Marquis GB (2014) Fatigue design of axially-loaded high frequency mechanical impact treated welds by the effective notch stress method. *Mater Des* 58:543–550
8. P. J. Haagenzen, S. J. Maddox, *IIW Recommendations on post weld improvement of steel and aluminum structures*, IIW document XIII-2200r4-07, revised February 2010
9. G. Nüsse, *REFRESH Lebensdauerverlängerung bestehender und neuer geschweißter Stahlkonstruktionen* (in German), Verlags und Vertriebsgesellschaft Forschungsvereinigung Stahlanwendungen, 2011
10. Le Quilliec G., Lieurade H.-P., Bousseau M., Drissi-Habti M., Inglebert G., Macquet P., Jubin L. (2011) *Fatigue behavior of welded joints treated by high frequency hammer peening: part i, experimental study*, iiw document xiii-2394-11
11. Tehrani YR, Ghahremani K (2013) Scott Walbridge: effect of quality control parameter variations on the fatigue performance of ultrasonic impact treated welds. *Int J Fatigue* 55:245–256
12. Berg J, Stranghoener N (2014) Fatigue strength of welded ultra high strength steels improved by high frequency hammer peening. *Procedia Materials Science* (3):71–76
13. Leitner M, Gerstbrein S, Ottersböck MJ, Stoschka M (2015) Fatigue strength of HFMI-treated high-strength steel joints under constant and variable amplitude block loading. *Procedia Engineering* 101:251–258
14. Lefebvre F, Revilla-Gomez C, Buffiere J-Y, Verdu C, Peyrac C (2014) Understanding the mechanism responsible for the beneficial effect of hammer peening in welded structure under fatigue loading. *Adv Mater Res* 996:761–768
15. A. Hobbacher (2008) Recommendations for the fatigue design of welded joints and components, International Institute of Welding, document IIW-1823-07 ex XIII-2151r4-07/XV-1254r4-07
16. Lihavainen V-M, Marquis GB (2006) Fatigue life estimation of ultrasonic impact treated welds using a local strain approach. *Steel Res Int* 77:896–900
17. Remes H (2013) Strain-based approach to fatigue crack initiation and propagation in welded steel joints with arbitrary notch shape. *Int J Fatigue* 52:114–123
18. Leitner M, Stoschka M, Eichlseder W (2014) Fatigue enhancement of thin-walled, high-strength steel joints by high-frequency mechanical impact treatment. *Weld World* 58:29–39
19. Mikkola E, Marquis G, Lehto P, Remes H, Hänninen H (2016) Material characterization of high-frequency mechanical impact (HFMI)-treated high strength steel. *Mater Des* 89:205–214
20. Mikkola E, Remes H, Marquis G (2017) A finite element study on residual stress stability and fatigue damage in high-frequency mechanical impact (HFMI)-treated welded joint. *Int J Fatigue* 94:16–29
21. V. Hardenacke, M. Farajian, D. Siegele, *Modelling and Simulation of High Frequency Mechanical Impact (HFMI) Treatment of Welded Joints*, IIW Document XIII-2533-14
22. G. Le Quilliec, H.-P. Lieurade, M. Bousseau, M. Drissi-Habti, G. Inglebert, P. Macquet, L. Jubin, *Fatigue Behavior of Welded Joints Treated by High Frequency Hammer Peening: Part II, Numerical Study*, IIW Document XIII-2395-11
23. Baptistaa R, Infante V, Branco C (2011) Fully dynamic numerical simulation of the hammer peening fatigue life improvement technique. *Procedia Engineering* 10:1943–1948
24. D. Simunek, M. Leitner, M. Stoschka, *Numerical simulation loop to investigate the local fatigue behaviour of welded and HFMI-treated joints*, IIW Document XIII-WG2-136-13
25. Guo C, Wang Z, Wang D, Hu S (2015) Numerical analysis of the residual stress in ultrasonic impact treatment process single-impact and two impact-models. *Appl Surf Sci* 347:596–601
26. J. Foehrenbach, V. Hardenacke, M. Farajian (2016) High frequency mechanical impact treatment (HFMI) for fatigue improvement: numerical and experimental investigations to describe the conditions in the surface layer, *Welding in the World*, July 2016, Volume 60, Issue 4, pp 749–755.
27. J. Foehrenbach (2015) Fatigue life prediction of high frequency mechanical impact treated welded joints by numerical simulation and damage mechanic approaches, Master Thesis, Offenburg University of Applied Science
28. Heitmann, H.; Vehoff, H.; Neumann, P. (1985) *Life prediction for random load fatigue based on the growth behaviour of microcrack*, Advances in Fracture Research (Hrsg.: Valluri, S. R.; et al.), Bd. 5, S. 3599–3606. Pergamon Press, Oxford
29. Neumann, P.; Heitmann, H.H.; Vehoff, H. (1985) *Schadensakkumulation bei statistischer Belastung* (in German), Ermüdungsverhalten metallischer Werkstoffe, pp. 167–184. DGM Informationsges. Verlag, Oberursel
30. Lawrence FV (1973) Estimation of fatigue crack propagation life in butt welds. *Welding J, Res Suppl* 53(5):212s–2220
31. Lawrence FV, Munse WH (1973) Fatigue crack propagation in butt welds containing joint penetration defects. *Welding J, Res Suppl* 52(5):221s–225s and 232
32. Lawrence F V, Mattos R J, Higashida Y and Burk J D (1978) 'Estimating the fatigue crack initiation life of welds', Fatigue Testing of Weldments, ASTM STP 648, Philadelphia Pa, ASTM, pp 134–158
33. Mattos R J and Lawrence F V (1977) 'Estimation of the fatigue crack initiation life in welds using low cycle fatigue concepts', SAE SP-424, Warrendale pa, SAE
34. Smith RN, Watson P, Topper TH (1970) A stress-strain function for the fatigue of metals. *J Mater* 5(4):767–778
35. J. A. Bannantine, D. F. Socie (1989) A variable amplitude Multiaxial Fatigue Life Prediction Method: Fatigue under Biaxial and Multiaxial Loading, Proc. Third International Conference on Biaxial Multiaxial Fatigue, Stuttgart. ESI Publication, London
36. Fatemi A, Socie DF (1988) A critical plane approach to multiaxial fatigue damage including out-of-phase loading. *Fatigue Fract Engng Mater Struct* 11(3):149–165
37. Roessle ML, Fatemi A (2000) Strain controlled fatigue properties of steels and some simple approximations. *Int J Fatigue* 22(6):495–511
38. D. F. Socie, G. Marquis (2000) Multiaxial Fatigue. Society of Automotive Engineers, illustrated edition
39. Shamsaei N, Fatemi A (2009) Effect of hardness on multiaxial fatigue behaviour and some simple approximations for steels. *Fatigue Fract Engng Mater Struct* 32:631–646
40. Sonats-ET, www.sonats-et.com
41. Harati, Ebrahim, et al. *Non-destructive measurement of weld toe radius using Weld Impression Analysis*, Laser Scanning Profiling and Structured Light Projection methods." First International Conference on Welding and Non Destructive Testing, Tehran, 2014
42. K. Ghahremani, M. Sara, J. Yaung, S. Walbridge, C. Haas, S. Dubois (2015) Quality assurance for high-frequency mechanical

- impact (HFMI) treatment of welds using handheld 3D laser scanning technology, *Welding in the World*, Vol. 59, No. 3
43. SYSWELD User manual
 44. Goldak J (1984) A finite element model for welding heat sources. *Metall Trans* 15:299–305
 45. 'J.-L. Chaboche, "A review of some plasticity and viscoplasticity constitutive theories," *International Journal of Plasticity*, 24, 1642–1693, 2008'; in addition, the following citation might be added: 'O. Muransky, C. Hamelin, M. Smith, P. Bendeich, L. Edwards, "The effect of plasticity theory on predicted residual stress fields in numerical weld analyses," *Computational Materials Science*, 54, 125–134, 2012
 46. Chaboche, J.L., *Cyclic viscoplastic constitutive equations*, Part I: A thermodynamically consistent formulation, *J. Appl. Mech.* 60, 1993, pp. 813–821. Part II: Stored energy – comparison between models and experiments, *J. Appl. Mech.* 60, 1993, pp. 822–828
 47. Lemaite J., Chaboche J. (1994) *Mechanics of solid materials*, Cambridge university press
 48. M. Farajian, T. Nitschke-Pagel, K. Dilger (2010) *Residual stress relaxation of quasi-statically and cyclically-loaded steel welds*, *welding in the world*, 54
 49. A. Dürr. *Zur Ermüdungsfestigkeit von Schweißkonstruktionen aus höherfesten Baustählen bei Anwendung von UIT-Nachbehandlung* (in German), PhD thesis, University of Stuttgart, Stuttgart, 2007
 50. I. Weich. *Ermüdungsverhalten mechanischer nachbehandelter Schweißverbindungen in Abhängigkeit des Randschichtzustandes* (in German). PhD thesis, Technical University of Carola-Wilhelmina, Braunschweig, 2008
 51. Sum W, Williams E, Leen S (2005) Finite element, critical-plane, fatigue life prediction of simple and complex contact configurations. *Int J Fatigue* 27:403–416
 52. Kocabicak U, Firat M (2004) A simple approach for multiaxial fatigue damage prediction based on FEM post-processing. *Mater Des* 25:73–82
 53. E. Haibach (2005) *Betriebsfestigkeit: Verfahren und Daten zur Bauteilberechnung* (in German), Springer Verlag, Berlin and Heidelberg and New York, 3rd corrected and supplemented edition edition
 54. Draper J (2007) *Modern fatigue life analysis*. ESI Publication, Warrington
 55. D. Radaj, C. M. Sonsino, and W. Fricke (2006) *Fatigue Assessment of Welded Joints by Local Approaches*, Woodhead Publishing Series in Welding and Other Joining Technologies. Elsevier Science, 2nd rev edition edition